Research article

Wenzhe Liu*, Lei Shi, Jian Zi and Che Ting Chan*

Ways to achieve efficient non-local vortex beam generation

https://doi.org/10.1515/nanoph-2021-0342
Received July 5, 2021; accepted September 2, 2021;
published online September 16, 2021

Abstract: Based on the insights into the phenomenon of bound states in the continuum, a novel approach utilizing the momentum-space polarization morphologies of periodic structures to generate vortex beams (VBs) has been proposed. Such periodic structures modulate beams in a nonlocal way and require no precise alignment. However, the efficiency of such an approach has not been analyzed in detail, and the efficiency in previous realizations is far from optimized. Here, we analyze the factors affecting the efficiency of nonlocal VB generation. We show that the maximal efficiency cannot exceed 25% if the periodic structure carries only singlet resonances. To go beyond this limit, we propose two approaches to improve efficiency. We theoretically analyze the mechanisms and verify the approaches by full-wave simulations. Both of the approaches serve to improve the generation efficiency by several folds.

Keywords: bound state in the continuum; Kerker effect; non-local; photonic crystal; polarization singularity; vortex beam.

1 Introduction

Vortex beams (VBs) are beams propagating in a spiral way, which have been shown to carry orbital angular momentum (OAM) [1–3]. In free space, the OAM carried by VBs is quantized due to the presence of the rotational symmetry [1]. In other words, VBs with different topological quantum numbers (or topological charges) are orthogonal to each other, making them promising candidates for enhancing the bandwidth of next-generation optical communications [4, 5]. VBs are also finding applications in many other fields such as optical microscopy [6], optical manipulation, and quantum optics [7]. Various structures, including spiral phase plates and meta-surfaces, have been proposed to generate VBs [8–14]. Recently, we propose a non-local approach to generate VBs, which is based on symmetry-protected bound states in continuum (BIC) in the momentum-space of periodic structures like photonic crystals [15]. The approach has the advantages of easy fabrication and alignment, but the generation efficiency by the cross-polarization conversion process is relatively low. In this paper, we analyze the factors affecting conversion efficiency. Considering those factors, we propose two approaches to enhance the efficiency, and we prove the validity of the two approaches using simulations.

2 Theory

2.1 Fundamental efficiency limit of previous studies

Previous studies [16–23] showed that both guided resonances in photonic structures and localized surface plasmon resonances in plasmonic structures can be decomposed into periodically aligned multipole moments so that the radiation and scattering behaviors can be understood from a more fundamental perspective. In such a perspective, symmetry-protected BICs and their topological polarization properties result from the symmetry-forced intensity poles of the multipole moments. For clarity and simplicity of this work, we also use dipole moment models to analyze the cross-polarized conversion efficiency.

To give an analytic explanation of the relatively low efficiency, we consider a case in which we applied singlet resonances of a periodically etched freestanding silicon nitride (Si_3N_4) slab to generate VBs [15]. Such a system has an up-down (z-direction) mirror symmetry and an in-plane rotational symmetry (usually cited as C_{nv} including C_{4v},

*Corresponding authors: Wenzhe Liu and Che Ting Chan, Department of Physics, The Hong Kong University of Science and Technology, Clear Water Bay, Kowloon, Hong Kong, China, E-mail: wzliu@ust.hk (W. Liu), phchan@ust.hk (C. T. Chan). https://orcid.org/0000-0002-6582-4161 (W. Liu). https://orcid.org/0000-0002-9335-8110 (C. T. Chan)
Lei Shi and Jian Zi, State Key Laboratory of Surface Physics, Key Laboratory of Micro- and Nano-Photonic Structures (Ministry of Education) and Department of Physics, Fudan University, Shanghai 200433, China, E-mail: lshi@fudan.edu.cn (L. Shi), jzi@fudan.edu.cn (J. Zi). https://orcid.org/0000-0001-8458-3941 (L. Shi). https://orcid.org/0000-0003-4131-4236 (J. Zi)

etc.) Considering the symmetry, the guided resonances applied to generate VBs can be viewed as generated by the collective excitation of an array of "vertical" multipole moments in the structure plane [21, 23]. We take electric dipole moments as an example, plotted as the left panel of Figure 1.

In the momentum space, the arrayed electric dipole moments shown in the left panel of Figure 1 will form a "node"-type (or "source/sink"-type) polarization morphology, with a BIC at the center (Γ point) which has a winding number of +1 [23–26]. A VB with topological charge ±2 can be generated accordingly [15]. With a temporal coupled mode theory (TCMT) [27] considering one resonance and four scattering channels, we can write down the transmission coefficient matrix of a resonance with specific in-plane wave vector $\mathbf{k}_{\parallel}$ in the spherical ($\hat{p}$-$\hat{s}$) frame:

$$\mathbf{T}_{p,s}(\mathbf{k}_{\parallel}) = \begin{pmatrix} t_{pp} & t_{ps} \\ t_{sp} & t_{ss} \end{pmatrix} = \begin{pmatrix} t_p & 0 \\ 0 & t_s \end{pmatrix} - \begin{bmatrix} \frac{|d_p|^2(t_p - r_p)}{\gamma_0 - i(\omega - \omega_0)} & \frac{d_p d_s^*(t_s - r_s)}{\gamma_0 - i(\omega - \omega_0)} \\ \frac{d_s d_p^*(t_p - r_p)}{\gamma_0 - i(\omega - \omega_0)} & \frac{|d_s|^2(t_s - r_s)}{\gamma_0 - i(\omega - \omega_0)} \end{bmatrix}. \quad (1)$$

Here, ω_0 and γ_0 are the real and imaginary parts of the $\mathbf{k}_{\parallel}$-dependent eigenfrequency of the applied collective resonance, while ω is the source frequency. (d_p, d_s) is the far-field polarization state vector of the resonance, in which $d_{p,s}$ are the coupling coefficients of the resonance to the free space through the two radiation channels of p and s polarization. $t_{p,s}$ and $r_{p,s}$ are the direct transmission and reflection coefficients, respectively. This matrix $\mathbf{T}_{p,s}$ can be viewed as a Jones matrix showing the structure's influence on the transmitting light.

Considering a small $\mathbf{k}_{\parallel}$, the difference between the direct transmission (reflection) coefficients of different polarizations $t_{p,s}$ ($r_{p,s}$) can be neglected. Consequently, the matrix becomes

$$\mathbf{T}_{p,s}(\mathbf{k}_{\parallel}) = t\mathbf{I} - \frac{t - r}{\gamma_0 - i(\omega - \omega_0)} \begin{pmatrix} |d_p|^2 & d_p d_s^* \\ d_s d_p^* & |d_s|^2 \end{pmatrix}, \quad (2)$$

by replacing the scattering coefficients with t and r ($\mathbf{I}$ here is the identity matrix). After a coordinate transformation, we obtain the matrix in the global Cartesian frame (x, y, z),

$$\mathbf{T}_{x,y}(\mathbf{k}_{\parallel}) = t\mathbf{I} - \frac{t - r}{\gamma_0 - i(\omega - \omega_0)} \begin{pmatrix} \tilde{d}_x{}^2 & \tilde{d}_x \tilde{d}_y \\ \tilde{d}_y \tilde{d}_x & \tilde{d}_y{}^2 \end{pmatrix}, \quad (3)$$

where $\tilde{d}_x, \tilde{d}_y$ are the real amplitudes of the correspondingly transformed coupling coefficients. Here, because polarization states are almost linear in the vicinity of the at-Γ BIC, the complex coupling coefficients of the polarization states shall have almost the same phase factor. As a

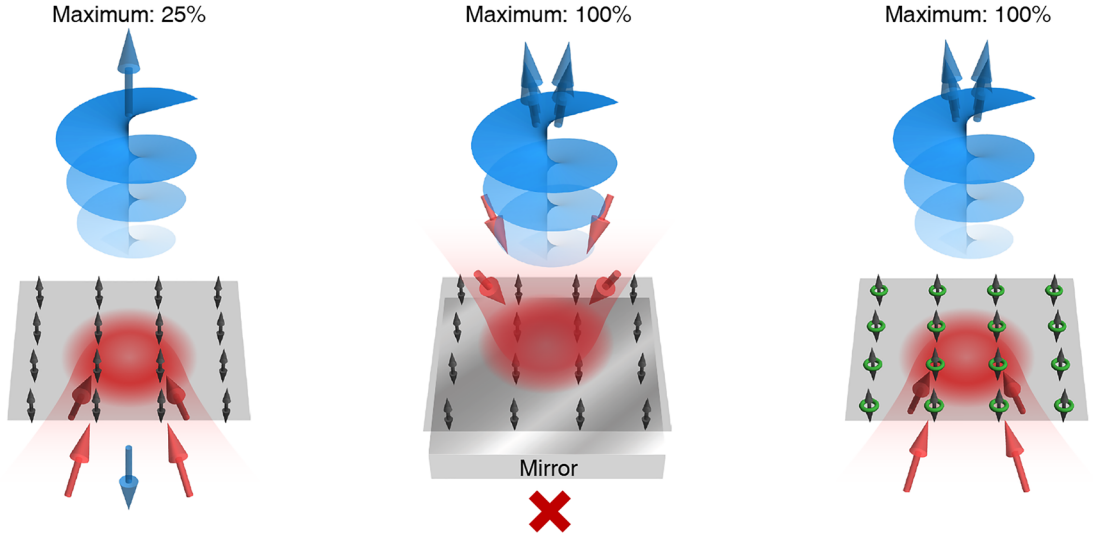

Figure 1: Mechanism to enhance the efficiency of nonlocal vortex beam generation. Left: Vortex generation using an array of single resonances. Vertical dipole resonances (black double-headed arrows) result in an at-Γ BIC and a corresponding polarization singularity in the momentum space, which can be applied to generate vortex beams. Red and blue colors correspond to the handedness of light. The maximal conversion efficiency for a specific wave vector is bounded by 25% for transmission (or reflection). Part of the incident power will be lost due to scattering in the opposite direction and direct transmission (reflection) without interacting with the resonances. Middle: Vortex generation by single resonances and a perfect mirror. The transmission channel is blocked by the mirror, and the cross-polarization conversion ratio can approach 100%. Right: Vortex generation enabled by dual resonances. Vertical electric dipole resonances are degenerate with vertical magnetic dipole resonances (green rings). The interference between the two kinds of resonances can greatly enhance the scattering on one side of the structure, improving the vortex generating efficiency.

result, the phase factor is eliminated in Eq. (3). Expressed using the helical basis $|\mathrm{CW}, \mathrm{CCW}\rangle$ (CW stands for clockwise polarization in the Cartesian frame while CCW stands for counterclockwise polarization), the matrix will be

$$\begin{aligned}\mathbf{T}_{\mathrm{heli}}(\mathbf{k}_{\parallel}) &= t\mathbf{I} - \frac{1}{2}\frac{\gamma_0(t-r)}{\gamma_0 - i(\omega-\omega_0)}\begin{pmatrix} 1 & \mathrm{e}^{2i\theta} \\ \mathrm{e}^{-2i\theta} & 1 \end{pmatrix} \\ &= t\mathbf{I} - \frac{1}{2}\frac{\gamma_0(t-r)}{\gamma_0 - i(\omega-\omega_0)}\mathbf{I} \\ &\quad - \frac{1}{2}\frac{\gamma_0(t-r)}{\gamma_0 - i(\omega-\omega_0)}\begin{pmatrix} 0 & \mathrm{e}^{2i\theta} \\ \mathrm{e}^{-2i\theta} & 0 \end{pmatrix}. \end{aligned} \tag{4}$$

We apply the condition of energy conservation $|d_x|^2 + |d_y|^2 = \gamma_0$ here, and θ is the azimuthal angle of the polarization state vector. The antidiagonal terms in Eq. (4) give the geometric phase caused by the cross-polarization conversion process of a circularly polarized incidence interacting with the momentum-space polarization states. Meanwhile, the conversion efficiency at $\mathbf{k}_{\parallel}$ is given by

$$\begin{aligned}\tau_{\mathrm{cross-pol.}}(\mathbf{k}_{\parallel}) &= \left|\frac{1}{2}\frac{\gamma_0(t-r)}{\gamma_0 - i(\omega-\omega_0)}\right|^2 \\ &= \frac{1}{4}\frac{\gamma_0^2(1 - rt^* - tr^*)}{\gamma_0^2 + (\omega-\omega_0)^2} \\ &= \frac{1}{4}\frac{\gamma_0^2}{\gamma_0^2 + (\omega-\omega_0)^2}, \end{aligned} \tag{5}$$

where we apply the relation $|r|^2 + |t|^2 = |r - t| = 1$ [27]. Equation (5) is a typical Lorentzian function in the frequency domain. Its maximum is 25% and occurs at $\omega = \omega_0$ (the on-resonance condition). As a conclusion, the cross-polarization conversion efficiency of a specific resonance at $\mathbf{k}_{\parallel}$ cannot exceed 25% for any singlet resonance of any freestanding structure with the mentioned symmetries.

Furthermore, for a real incident beam, it contains different $\mathbf{k}_{\parallel}$ components. The overall conversion efficiency of the whole beam is determined by how well the high conversion efficiency region overlaps with the momentum-space beam profile at a specific wavelength. Clearly, the $\mathbf{k}_{\parallel}$-dependent efficiency can hardly stay at the maximum throughout the momentum-space range covered by the beam. The more wave-vector-dispersive the applied resonance is the less area the high-efficiency region can cover, and the less overall efficiency we get. For guided resonances, the high-efficiency region is usually a thin ring surrounding the center of the momentum space. Meanwhile, the incident beam usually appears as a Gaussian spot at the center of the momentum space. As a result of the mismatch in the covered region, a large amount of the power is not converted, making the overall efficiency low.

The above discussion applies to the reflection of the system as well. All these factors together give a relatively low efficiency in the previous implementation of such ideas. The question is, can the overall efficiency be improved? From the $\mathbf{k}_{\parallel}$-dependence aspect, the problem can somehow be solved in two ways. One is to engineer the momentum-space dispersion ($\mathbf{k}_{\parallel}$ dependence of ω_0 and γ_0) of the resonance. A flattened dispersion can keep the efficiency high by providing a larger range usable in the momentum space. The other is to engineer the beam: a Bessel-like beam whose momentum-space coverage is also a ring will obviously loosen the requirement on the $\mathbf{k}_{\parallel}$-dependent efficiency. But, more importantly, can we break the fundamental 25% limit?

2.2 Enhancing the conversion efficiency: the mirror approach

We now discuss two mechanisms to break the limit. If we take a deeper look at the above system as shown in the left panel of Figure 1, we see that quite a large amount of the incident power is lost to the other outgoing channels, especially the scattering channels in the opposite direction. If those channels can be blocked, the efficiency may be enhanced. An intuitive way is to use a perfect mirror to cover one side of the structure, as shown in the middle panel of Figure 1. In such a case, the energy conservation condition becomes $d_x^2 + d_y^2 = 2\gamma_0$. If no transmission happens, we have $t = 0$ and $|r| = 1$. Therefore, with some simple modifications on Eq. (5) we can get

$$\begin{aligned}\tau^{\mathrm{mirror}}_{\mathrm{cross-pol.}}(\mathbf{k}_{\parallel}) &= \left|\frac{1}{2}\frac{2\gamma_0 r}{\gamma_0 - i(\omega-\omega_0)}\right|^2 \\ &= \frac{\gamma_0^2}{\gamma_0^2 + (\omega-\omega_0)^2}. \end{aligned} \tag{6}$$

Clearly, the maximal conversion efficiency can be increased to 100% with the perfect mirror introduced. This approach seems very simple. However, it only works in a reflective geometry, making the approach less useful in practical applications. Moreover, perfect mirrors are only available in specific frequency ranges, e.g. radio frequencies. In the optical range, metallic mirrors are inevitably absorptive, which can reduce efficiency. One can mitigate the loss impact by moving the field hotspots away from the lossy mirror.

2.3 Enhancing the conversion efficiency: the dual-resonance approach

To realize better efficiency without blocking the transmission, we need to consider some other mechanisms. Instead

of applying a perfect mirror, another resonance that is degenerate with the existing resonance can be introduced. The interference between the two resonances enables us to prevent the power from scattering into the unwanted channels and distribute the power to the desired one(s). From the viewpoint of multipole moments, such a phenomenon is a Kerker effect [20, 28–30]. Note that we want to improve the overall efficiency over the momentum space, and hence a ring-like degeneracy in the momentum space (i.e., a nodal ring) is necessary. In the meantime, the introduced multipole moment shall have the same winding number as the existing one in order to ensure stable interference along the nodal ring. In our example, illustrated in the right panel of Figure 1, we can introduce an array of vertical magnetic dipole moments. The electric dipoles are odd about the mirror plane, while the magnetic ones are even. Such a symmetry guarantees the orthogonality of the two kinds of dipole moments and accordingly the existence of the nodal line. Both the two dipole moments have the same polarization winding number of +1.

Analytically, we apply a TCMT with two resonances and four scattering channels [27] to get the expressions of the transmission coefficients which will be

$$\mathbb{T}_{p,s}(\mathbf{k}_\parallel)=\begin{bmatrix} t_p-\dfrac{(t_p-r_p)\ |d_0^p|^2}{\gamma_0-i(\omega-\omega_0)}-\dfrac{(t_p+r_p)\ |d_1^p|^2}{\gamma_1-i(\omega-\omega_1)} & -\dfrac{d_0^p d_0^{s*}(t_s-r_s)}{\gamma_0-i(\omega-\omega_0)}-\dfrac{d_1^p d_1^{s*}(t_s+r_s)}{\gamma_1-i(\omega-\omega_1)} \\ -\dfrac{d_0^s d_0^{p*}(t_p-r_p)}{\gamma_0-i(\omega-\omega_0)}-\dfrac{d_1^s d_1^{p*}(t_p+r_p)}{\gamma_1-i(\omega-\omega_1)} & t_s-\dfrac{(t_s-r_s)\ |d_0^s|^2}{\gamma_0-i(\omega-\omega_0)}-\dfrac{(t_s+r_s)\ |d_1^s|^2}{\gamma_1-i(\omega-\omega_1)} \end{bmatrix}. \tag{7}$$

Here, subscript "0" refers to the electric dipole moments, and subscript "1" refers to the magnetic dipoles. We make the two resonances degenerate and only consider the on-resonance cases, so $\omega_0=\omega_1=\omega$. Again, we apply the approximation $(r,t)_{p,s}\approxeq(r,t)$ and assume linear polarization states by considering a small $\mathbf{k}_\parallel$, and after coordinate and basis transformations we have

$$\begin{aligned}\mathbb{T}_{\text{heli}}(\mathbf{k}_\parallel)=t\mathbf{I}&-\frac{1}{2}\frac{\gamma_0(t-r)}{\gamma_0}\begin{pmatrix}1 & e^{2i\theta_0}\\ e^{-2i\theta_0} & 1\end{pmatrix}\\ &-\frac{1}{2}\frac{\gamma_1(t+r)}{\gamma_1}\begin{pmatrix}1 & e^{2i\theta_1}\\ e^{-2i\theta_1} & 1\end{pmatrix}\\ =&-\frac{1}{2}(t-r)\begin{pmatrix}0 & e^{2i\theta_0}\\ e^{-2i\theta_0} & 0\end{pmatrix}\\ &-\frac{1}{2}(t+r)\begin{pmatrix}0 & e^{2i\theta_1}\\ e^{-2i\theta_1} & 0\end{pmatrix}.\end{aligned} \tag{8}$$

From Eq. (8), we find that the co-polarized transmission has already been eliminated by introducing the orthogonal magnetic resonance. Assuming that the far-field polarization azimuthal angle θ_1 of the introduced magnetic dipoles always differs from the one of the electric dipoles (θ_0) by a constant angle Δ, we have

$$\begin{aligned}\mathbb{T}_{\text{heli}}(\mathbf{k}_\parallel)=&-\frac{1}{2}\begin{pmatrix}0 & e^{2i\theta_0}\\ e^{-2i\theta_0} & 0\end{pmatrix}\\ &\begin{bmatrix}t-r+(t+r)e^{-2i\Delta} & 0\\ 0 & t-r+(t+r)e^{2i\Delta}\end{bmatrix}.\end{aligned} \tag{9}$$

Interestingly, the cross-polarization conversion efficiency is no longer symmetric for the CW-to-CCW and the CCW-to-CW cases here. The on-resonance conversion efficiency $\tau^{\text{dual}}_{\text{cross-pol.}}(\mathbf{k}_\parallel)$ for the former case will be

$$\begin{aligned}&\frac{1}{2}\left[|t|^2(1+\cos\,2\Delta)+|r|^2(1-\cos\,2\Delta)\right]\\ &\qquad-\left[\frac{i}{2}(rt^*-tr^*)\sin\,2\Delta\right],\end{aligned} \tag{10}$$

while the efficiency of the latter case will be

$$\begin{aligned}&\frac{1}{2}\left[|t|^2(1+\cos\,2\Delta)+|r|^2(1-\cos\,2\Delta)\right]\\ &\qquad+\left[\frac{i}{2}(rt^*-tr^*)\sin\,2\Delta\right].\end{aligned} \tag{11}$$

The electromagnetic field of the introduced magnetic dipole moments is also orthogonal to the field of the existing electric dipole moments in the structure plane in our

example. Consequently, Δ can be taken as $\pi/2$. We find that the conversion efficiencies for both cases become the same again, which is $|r|^2$. It is surprising that the on-resonance conversion efficiency ceases to be a constant, but is rather determined by the direct scattering coefficient(s). This allows us to break the constant limit of 25%, as long as the direct reflectance is high enough. Because we take advantage of degenerate electric and magnetic dipole resonances in this approach, we would like to call it a "dual-resonance" approach.

Note that, such an approach can be applied in enhancing either the transmissive conversion efficiency or the reflective one by tuning the direct reflectance and transmittance. When $|r|^2 = 0$ and $|t|^2 = 1$, the transmissive conversion is eliminated and all the power is routed to the reflective conversion. In the optical range, $|r|^2 = 1$ may be difficult to achieve with a single-layered dielectric photonic crystal slab, and therefore a transmissive generation setup may require a multi-layered structure. On the other hand, $|r|^2 = 0$ can be easily achieved with thin-film interference to realize reflective vortex beam generation without absorptive mirrors.

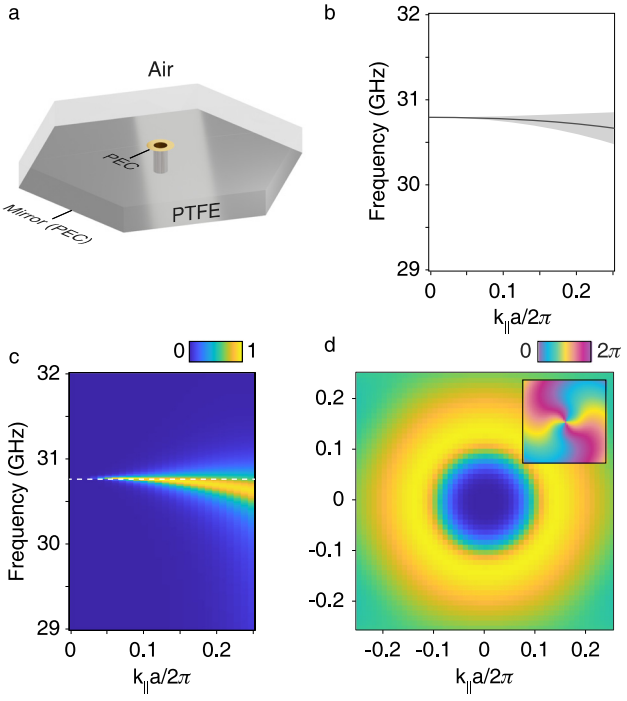

Figure 2: An example of the mirror approach.
(a) The schematic view of a unit cell of the structure. A perfect-electric-conductor (PEC) coated via hole is punched in a dielectric slab, of which the bottom is covered by a PEC layer acting as a perfect mirror. (b) The dispersion of the applied resonance is supported by the structure. The solid line marks the real part of the eigenfrequencies, while the accompanying transparent shade marks the imaginary part. The via hole act as a vertical electric dipole, which leads to a symmetry-protected BIC at $\mathbf{k}_{\parallel} = 0$. (c) The calculated cross-polarization conversion efficiency (reflectance). On-resonance efficiency approaches 100%. (d) The cross-polarization conversion efficiency mapped at the frequency of 30.75 GHz [marked out by a white dashed line in (c)]. The efficiency map shares the same color map of (c). The inset shows the phase map after a CW-to-CCW cross-polarization conversion, which has a topological charge of −2.

3 Simulation demonstrations

In order to demonstrate the validity of the two proposed approaches, we design structures operating in the microwave range and perform simulations. For the mirror approach, the structure is chosen to be a dielectric slab [made of polytetrafluoroethylene (PTFE), $\epsilon_r \sim 2.1$] in which a hexagonal array of via holes is etched, as illustrated in Figure 2(a). The bottom of the slab and the inner wall of the holes are coated with a perfect electric conductor (PEC) layer. The distance between two holes, i.e., the lattice constant a, is 0.540 cm. The thickness of the slab is 0.122 cm, and the radius of the holes is chosen to be 0.016 cm. The width of the PEC strips around the via hole is 0.030 cm. The via holes and the PEC mirror together work as resonators supporting vertical electric dipole moments.

Using full-wave simulations, we obtain the dispersion of the electric dipole resonance, shown in Figure 2(b). The dispersion of such a local resonance is flat enough so that the overall efficiency over the momentum space is improved. One can clearly see the existence of a BIC at the Γ point from the plotted imaginary part of eigenfrequencies. The $\mathbf{k}_{\parallel}$-dependent cross-polarization conversion efficiency is calculated and plotted in Figure 2(c). For each $\mathbf{k}_{\parallel}$, a Lorentzian line shape whose maximum approaches 100% can be seen, as we have predicted above. Although the wave-vector range is not very small in this example, the assumptions in our discussion [$(r,t)_{p,s} \approxeq (r,t)$ and linear polarization states] are still valid, discussed in Supplementary Information. Choosing the operating frequency to be 30.75 GHz, the momentum-space conversion efficiency distribution is mapped as Figure 2(d). If a Gaussian beam with a $\sim$ 15.7-degree divergence angle is shined onto the structure, the overall reflecting conversion efficiency reaches $\sim$ 46%, which will be about four times the efficiency using a singlet resonance. Correspondingly, the phase after CCW analyzing under a CW incidence is shown in the inset of Figure 2(d). We can observe an obvious phase vortex of topological charge −2.

On the other hand, the dual-resonance approach requires a more complex structure, which supports both electric and magnetic dipole resonances. In Figure 3(a),

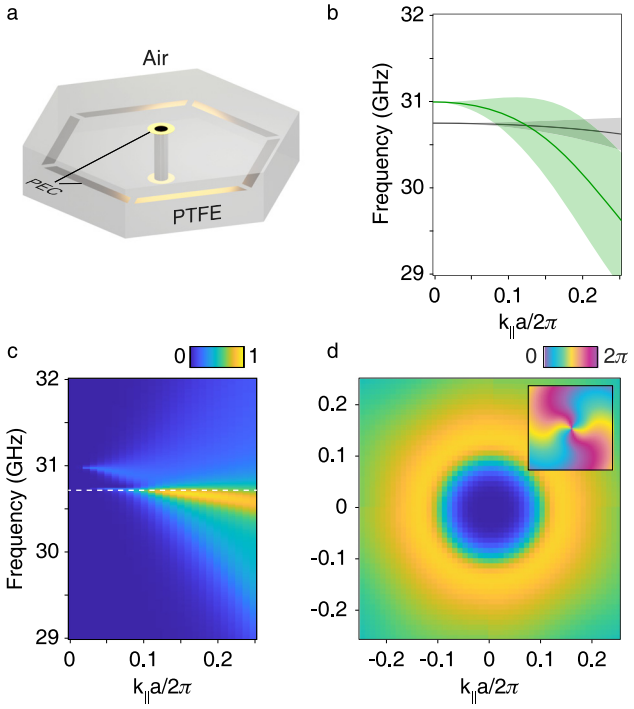

Figure 3: An example of the dual-resonance approach. (a) The schematic view of a unit cell of the structure. A PEC coated via hole is punched through the dielectric slab, and a hexagonal split ring resonator with six slits is put at the center of the slab. (b) The dispersions of the applied resonances are supported by the structure. The solid lines mark the real part of the eigenfrequencies, while the accompanying shades mark the imaginary part. The black curve corresponds to the vertical electric dipole resonance supported by the via hole, while the green curve corresponds to the vertical magnetic dipole resonance supported by the split ring resonator. (c) The calculated cross-polarization conversion efficiency (transmittance). On-resonance efficiency exceeds 90% when the two resonances become nearly degenerate. (d) The cross-polarization conversion efficiency mapped at the frequency of 30.71 GHz [marked out by a white dashed line in (c)]. The efficiency map shares the same color map of (c). The inset shows the phase map after a CW-to-CCW cross-polarization conversion, which has a topological charge of −2.

we illustrate the unit cell of the designed structure. The dielectric slab and the via holes are retained, but the PEC mirror is now removed. The thickness of the slab with the via holes punched through is doubled (0.244 cm) in order to support a similar electric dipole resonance to the one in the former approach. An array of hexagonal split-ring resonators is added to the central plane of the slab. The in-plane winding current along the patches of the split-ring resonator introduces the required vertical magnetic dipole resonance. Moreover, the ring resonator array acts as a Faraday shield. The patches added have the same width as the PEC strip around the via hole, and their length is 0.273 cm. Slits between the patches are 0.015 cm wide. With the direct transmittance suppressed to almost zero by the Faraday shielding effect, the introduced magnetic dipole moments along with the existing electric dipole moments can greatly improve the conversion efficiency.

From Figure 3(b), we can see the calculated dispersions of the two resonances. As the structure has the up-down mirror symmetry, the dispersions of the electric and magnetic resonances directly cross each other at $\mathbf{k}_{\parallel} \sim 0.125 \cdot 2\pi/a$, resulting in a nodal ring. Two BICs are observed from the plotted imaginary part of the eigenfrequencies. As expected, in the $\mathbf{k}_{\parallel}$ region where the two dispersions are nearly degenerate, the transmitting conversion efficiency is lifted to over 90% (∼93%), as shown in Figure 3(c). At 30.71 GHz, the conversion efficiency map is plotted as Figure 3(d), of which the inset shows the phase map in the CW-to-CCW-conversion case. The overall transmitting conversion efficiency at 30.71 GHz under a Gaussian beam incidence whose divergence angle is ∼15.7 degrees is calculated to be about 42%, ∼3.7 times the efficiency using a single resonator.

From the results, we can see that both approaches work well. The mirror approach can in principle reach a maximal efficiency of 100%. The structure and the corresponding dispersion are very simple. However, in realistic applications, perfect mirrors are difficult to construct. If the material loss is considered, fine tuning of the structure is necessary to reduce on-resonance absorption. Another disadvantage of this approach is that it only works in reflective setups. The dual-resonance approach, on the other hand, does not require a mirror but involves two orthogonal multipole resonances. Utilizing the interference between degenerate resonances, directional cross-polarized scattering can happen, and high conversion efficiency can be realized in a transmissive (or reflective) setup. The structure still needs to be carefully designed so that the two orthogonal resonances can be degenerate in the desired momentum-space region. Besides, the direct transmittance and reflectance will determine the transmitting conversion efficiency, and thus the design shall take the direct scattering process into consideration as well. The two approaches work in any frequency range in principle. However, if one wants to apply the approaches in the optical range, complex structures may be necessary since lossless metal does not exist in this wavelength range.

4 Conclusion

We propose two approaches to improve the cross-polarization efficiency of nonlocal VB generation. One is

based on a perfect mirror, and the other is based on dual resonances. Both approaches are verified with simulations, which show an enhancement in efficiency by several folds. The theory can be applied to all types of structures and can be extended to systems whose polarization basis is not the helical one. High conversion efficiency can improve the usability of periodic structures as non-local beam modulators and other promising applications such as nonlocal nonlinear vortex generation [31–33] can be expected.

Author contribution: All the authors have accepted responsibility for the entire content of this submitted manuscript and approved submission.

Research funding: This work is supported by Hong Kong Research Grants Council through grant N_HKUST608/17 and the Croucher Foundation (CAS20SC01). Lei Shi was further supported by the National Natural Science Foundation of China (11774063 and 11727811).

Conflict of interest statement: The authors declare no conflicts of interest regarding this article.

References

[1] L. Allen, M. W. Beijersbergen, R. J. C. Spreeuw, and J. P. Woerdman, "Orbital angular momentum of light and the transformation of Laguerre-Gaussian laser modes," *Phys. Rev. A*, vol. 45, pp. 8185–8189, 1992.

[2] K. Y. Bliokh, "Geometrical optics of beams with vortices: berry phase and orbital angular momentum hall effect," *Phys. Rev. Lett.*, vol. 97, p. 043901, 2006.

[3] M. R. Dennis, K. O'Holleran, and M. J. Padgett, "Chapter 5 singular optics: optical vortices and polarization singularities," in *Progress in Optics*, vol. 53, Amsterdam, Elsevier, 2009, pp. 293–363.

[4] G. Walker, A. S. Arnold, and S. Franke-Arnold, "Trans-spectral orbital angular momentum transfer via four-wave mixing in Rb vapor," *Phys. Rev. Lett.*, vol. 108, p. 243601, 2012.

[5] A. E. Willner, H. Huang, Y. Yan, et al., "Optical communications using orbital angular momentum beams," *Adv. Opt. Photon.*, vol. 7, pp. 66–106, 2015.

[6] S. Fürhapter, A. Jesacher, S. Bernet, and M. Ritsch-Marte, "Spiral interferometry," *Opt. Lett.*, vol. 30, pp. 1953–1955, 2005.

[7] A. Mair, A. Vaziri, G. Weihs, and A. Zeilinger, "Entanglement of the orbital angular momentum states of photons," *Nature*, vol. 412, pp. 313–316, 2001.

[8] M. Beijersbergen, R. Coerwinkel, M. Kristensen, and J. Woerdman, "Helical-wavefront laser beams produced with a spiral phaseplate," *Opt. Commun.*, vol. 112, pp. 321–327, 1994.

[9] Z. Bomzon, G. Biener, V. Kleiner, and E. Hasman, "Space-variant pancharatnam–berry phase optical elements with computer-generated subwavelength gratings," *Opt. Lett.*, vol. 27, pp. 1141–1143, 2002.

[10] A. V. Kildishev, A. Boltasseva, and V. M. Shalaev, "Planar photonics with metasurfaces," *Science*, vol. 339, p. 1232009, 2013.

[11] N. Yu and F. Capasso, "Flat optics with designer metasurfaces," *Nat. Mater.*, vol. 13, pp. 139–150, 2014.

[12] E. Karimi, S. A. Schulz, I. De Leon, H. Qassim, J. Upham, and R. W. Boyd, "Generating optical orbital angular momentum at visible wavelengths using a plasmonic metasurface," *Light Sci. Appl.*, vol. 3, p. e167, 2014.

[13] D. Lin, P. Fan, E. Hasman, and M. L. Brongersma, "Dielectric gradient metasurface optical elements," *Science*, vol. 345, pp. 298–302, 2014.

[14] P. Miao, Z. Zhang, J. Sun, et al., "Orbital angular momentum microlaser," *Science*, vol. 353, pp. 464–467, 2016.

[15] B. Wang, W. Liu, M. Zhao, et al., "Generating optical vortex beams by momentum-space polarization vortices centred at bound states in the continuum," *Nat. Photon.*, vol. 14, pp. 623–628, 2020.

[16] J. D. Jackson, *Classical Electrodynamics*, Hoboken, John Wiley & Sons, 1962.

[17] C. F. Bohren and D. R. Huffman, *Absorption and Scattering of Light by Small Particles*, Hoboken, Wiley, 1998.

[18] A. Doicu, T. Wriedt, and Y. A. Eremin, *Light Scattering by Systems of Particles*, vol. 124, Berlin, Heidelberg, Springer, 2006.

[19] D. A. Powell, "Interference between the modes of an all-dielectric meta-atom," *Phys. Rev. Appl.*, vol. 7, p. 034006, 2017.

[20] W. Liu and Y. S. Kivshar, "Generalized Kerker effects in nanophotonics and meta-optics [Invited]," *Opt. Express*, vol. 26, pp. 13085–13105, 2018.

[21] A. A. Bogdanov, K. L. Koshelev, P. V. Kapitanova, et al., "Bound states in the continuum and fano resonances in the strong mode coupling regime," *Adv. Photon.*, vol. 1, p. 016001, 2019.

[22] W. Chen, Y. Chen, and W. Liu, "Multipolar conversion induced subwavelength high-q Kerker supermodes with unidirectional radiations," *Laser Photon. Rev.*, vol. 13, p. 1900067, 2019.

[23] W. Chen, Y. Chen, and W. Liu, "Singularities and poincaré indices of electromagnetic multipoles," *Phys. Rev. Lett.*, vol. 122, p. 153907, 2019.

[24] B. Zhen, C. W. Hsu, L. Lu, A. D. Stone, and M. Soljačić, "Topological nature of optical bound states in the continuum," *Phys. Rev. Lett.*, vol. 113, p. 257401, 2014.

[25] Y. Zhang, A. Chen, W. Liu, et al., "Observation of polarization vortices in momentum space," *Phys. Rev. Lett.*, vol. 120, p. 186103, 2018.

[26] H. M. Doeleman, F. Monticone, W. den Hollander, A. Alù, and A. F. Koenderink, "Experimental observation of a polarization vortex at an optical bound state in the continuum," *Nat. Photon.*, vol. 12, pp. 397–401, 2018.

[27] S. Fan, W. Suh, and J. Joannopoulos, "Temporal coupled-mode theory for the fano resonance in optical resonators," *J. Opt. Soc. Am. A*, vol. 20, pp. 569–572, 2003.

[28] M. Kerker, D. S. Wang, and C. Giles, "Electromagnetic scattering by magnetic spheres," *J. Opt. Soc. Am.*, vol. 73, pp. 765–767, 1983.

[29] P. Jin and R. W. Ziolkowski, "Metamaterial-inspired, electrically small Huygens sources," *IEEE Antennas Wirel. Propag. Lett.*, vol. 9, pp. 501–505, 2010.
[30] C. Pfeiffer and A. Grbic, "Metamaterial huygens' surfaces: tailoring wave fronts with reflectionless sheets," *Phys. Rev. Lett.*, vol. 110, p. 197401, 2013.
[31] G. Li, M. Kang, S. Chen, et al., "Spin-enabled plasmonic metasurfaces for manipulating orbital angular momentum of light," *Nano Lett.*, vol. 13, pp. 4148–4151, 2013.
[32] G. Li, L. Wu, K. F. Li, et al., "Nonlinear metasurface for simultaneous control of spin and orbital angular momentum in second harmonic generation," *Nano Lett.*, vol. 17, pp. 7974–7979, 2017.
[33] B. Liu, B. Sain, B. Reineke, et al., "Nonlinear wavefront control by geometric-phase dielectric metasurfaces: influence of mode field and rotational symmetry," *Adv. Opt. Mater.*, vol. 8, p. 1902050, 2020.

Supplementary Material: The online version of this article offers supplementary material (https://doi.org/10.1515/nanoph-2021-0342).